*J. Fluid Mech.* (1997), *vol.* 335, *pp.* 57–73



# On the long-wave instability of natural-convection boundary layers

By P. G. DANIELS[1] AND JOHN C. PATTERSON[2]†

[1] Department of Mathematics, City University, Northampton Square, London EC1V 0HB, UK

[2] Centre for Water Research, University of Western Australia, Nedlands W.A. 6009, Australia

(Received 26 October 1995 and in revised form 22 October 1996)

This paper considers the stability of the one-dimensional boundary layer generated by sudden heating of an infinite vertical wall. A quasi-steady approximation is used to analyse the asymptotic form of the lower branch of the neutral curve, corresponding to disturbances of wavelength much greater than the boundary-layer width. This leads to predictions of the critical wavenumber for neutral stability and the maximum phase speed of the travelling waves. Results are obtained for a range of Prandtl numbers and are compared with solutions of the full stability equations and with numerical simulations and experimental observations of cavity flows driven by sudden heating of the sidewalls.

## 1. Introduction

The flow induced adjacent to a vertical wall heated above the ambient temperature is one of the fundamental heat and mass transfer mechanisms and has therefore a wide application in industrial and geophysical heat transfer problems. The classical one-dimensional solutions for the suddenly heated doubly infinite plate in a stationary isothermal fluid have been available for many years, for a variety of thermal boundary conditions including the sudden application of a constant or varying heat flux or temperature at the wall (e.g. Goldstein & Briggs 1964). The steady flow adjacent to a heated semi-infinite plate has been described using a similarity transformation of the usual boundary-layer equations (Ostrach 1964), and although closed-form solutions are not available, numerically generated solutions are well known.

Of particular interest is the development of this latter flow, which may be described as follows (Siegel 1958): at each fixed position downstream of the leading edge of the plate the flow initially develops as though the wall were doubly infinite with one-dimensional flow and temperature fields which depend only on the lateral distance from the wall. After some finite time has elapsed, the presence of the leading edge is felt, and a transition to the two-dimensional flow occurs. The transition may usually be observed as an oscillatory modulation of the temperature time series, and the passage of this transition region is usually referred to as the 'leading-edge effect'.

A number of studies have attempted to describe the transition process, but largely without success (e.g. Goldstein & Briggs 1964; Brown & Riley 1973; Ingham 1985). In general terms, these papers have failed to accurately predict the speed at which the transition region travels along the plate; in all cases this speed has been based on convective transport by the boundary-layer flow itself. In the Brown & Riley (1973) and Ingham (1985) papers, this assumption was supported by noting that the character

† Present address: Department of Civil and Systems Engineering, James Cook University, Townsville, Queensland 4811, Australia.

of the boundary-layer equations changed at a particular time for a given vertical position: this allowed an estimate of the speed of the effect as it travelled along the boundary layer. Ingham's (1985) numerical calculations of the boundary-layer solution for the constant temperature wall condition are in reasonable agreement with the analytical prediction of Brown & Riley (1973) but differ significantly from both full numerical simulations of the start-up flow in a side-heated cavity (Schladow 1990) and from recent experimental results obtained by Graham (1995). Likewise, for the constant-heat-flux wall condition the propagation speed observed in experiments by Mahajan & Gebhart (1978) and Joshi & Gebhart (1987) is up to as much as twice the speed predicted by analysis based on convective transport by the boundary layer. In order to address this discrepancy, Armfield & Patterson (1992) used a stability analysis of the developing, i.e., the one-dimensional, boundary layer, in the context of a contained cavity flow, to show that a much better estimate was obtained from the fastest phase speed of the spectrum of waves that travelled along the boundary layer following perturbation by the leading-edge singularity. This maximum phase speed occurred, for the case studied by Armfield & Patterson, at a wavenumber just less than the lowest neutral wavenumber, i.e., just on the decaying side of the left-hand branch of the neutral curve. Further, this model for the leading-edge effect also provided a mechanism for the oscillatory modulation of the signal in the form of the amplified group of travelling waves, and indeed the simulated and observed oscillations proved to have a wavenumber consistent with the maximally amplified waves obtained from the stability analysis.

This proposed connection between the leading-edge effect and the stability of the one-dimensional boundary layer focused attention on the need to provide a more detailed analysis of the stability properties of the boundary layer, and particularly of the properties at the low-wavenumber end of the spectrum of travelling waves. Although there have been a number of studies of various related configurations (e.g. Gill & Davey 1969; Gebhart & Mahajan 1982; Joshi & Gebhart 1987; Krane & Gebhart 1993), none of these addressed the particular problem of the low-wavenumber phase and group velocities and amplification properties. These stability studies naturally have a much wider application than to just the leading-edge effect, and there is a range of results over the whole wavenumber spectrum. In this paper, however, we focus on the small-wavenumber limit, and do not, except in passing, discuss the implication for the leading-edge effect.

In §2 the full stability problem is formulated, and the one-dimensional base flow and temperature fields are identified. The low-wavenumber limit is formulated in §3, and asymptotic and numerical methods are established for the solution of the reduced set of equations resulting from this limit in §4. The results from the numerical solutions are given in §5, and are compared with the numerical solution of the full set of equations in §6. In §7 we discuss the dependence of the results on the Prandtl number, and in §8 we consider some of the implications of these results and indicate how they will match with similar solutions at intermediate and high wavenumbers.

## 2. Formulation

The configuration under consideration is an infinite vertical plate, initially at temperature $T_0$ immersed in a stationary isothermal fluid, also at temperature $T_0$. At time $t = 0$, the temperature of the plate is instantaneously increased to $T_0 + \Delta T$, and maintained at that temperature. The full equations of motion describing the resulting motion and temperature fields are, with the usual Boussinesq assumption,

$$\frac{\partial u^*}{\partial x^*}+\frac{\partial v^*}{\partial y^*}=0, \tag{2.1}$$

$$\frac{\partial u^*}{\partial t^*}+u^*\frac{\partial u^*}{\partial x^*}+v^*\frac{\partial u^*}{\partial y^*}=-\frac{1}{\rho_0}\frac{\partial p^*}{\partial x^*}+\nu\nabla^2 u^*, \tag{2.2}$$

$$\frac{\partial v^*}{\partial t^*}+u^*\frac{\partial v^*}{\partial x^*}+v^*\frac{\partial v^*}{\partial y^*}=-\frac{1}{\rho_0}\frac{\partial p^*}{\partial y^*}+\nu\nabla^2 v^*+g\beta(T^*-T_0), \tag{2.3}$$

$$\frac{\partial T^*}{\partial t^*}+u^*\frac{\partial T^*}{\partial x^*}+v^*\frac{\partial T^*}{\partial y^*}=\kappa\nabla^2 T^*, \tag{2.4}$$

with
$$u^*=v^*=0, \quad T^*=T_0+\Delta T \quad \text{at} \quad x^*=0 \quad \text{for} \quad t^*>0, \tag{2.5}$$

$$u^*, v^*\to 0, \quad T^*\to T_0 \quad \text{as} \quad x^*\to\infty \quad \text{for} \quad t^*>0, \tag{2.6}$$

$$u^*=v^*=0, \quad T^*=T_0 \quad \text{for} \quad t^*\leqslant 0, \tag{2.7}$$

where $u^*, v^*$ are the velocities in the horizontal and vertical directions $x^*, y^*$ respectively, $t^*$ is the time, $p^*$ the pressure, $T^*$ the temperature, $\rho_0$ the density at temperature $T_0$, $\nu$ and $\kappa$ the kinematic viscosity and thermal diffusivity of the fluid respectively, $\beta$ the coefficient of thermal expansion and $g$ the acceleration due to gravity.

Non-dimensional variables are introduced by defining

$$\left.\begin{aligned} x^*=hx, \quad y^*=hy, \quad t^*=\frac{h^2}{\nu}t, \\ u^*=\frac{\nu}{h}u, \quad v^*=\frac{\nu}{h}v, \quad T^*=T_0+T\Delta T, \end{aligned}\right\} \tag{2.8}$$

where $h=(\nu\kappa/g\beta\Delta T)^{1/3}$ is a characteristic length scale. Substitution into (2.1)–(2.7) and elimination of the pressure yields a non-dimensional system for $u$, $v$ and $T$ which has an exact one-dimensional solution (Goldstein & Briggs 1964) with $u=0$ and

$$T=T_B(x,t)=F(\eta), \quad v=v_B(x,t)=tV(\eta), \tag{2.9}$$

where $\eta=x/t^{1/2}$ and for Prandtl numbers $Pr=\nu/\kappa\neq 1$,

$$F(\eta)=\operatorname{erfc}(Pr^{1/2}\eta/2), \tag{2.10}$$

$$V(\eta)=\frac{4}{Pr\,(Pr-1)}[i^2\operatorname{erfc}(\eta/2)-i^2\operatorname{erfc}(Pr^{1/2}\eta/2)], \tag{2.11}$$

where $i^2\operatorname{erfc}$ is the second integral of the complementary error function.

We examine the stability of this basic time-dependent state to small perturbations by writing

$$T=T_B(x,t)+\epsilon\,\mathrm{Re}\,[\tau(x)\,\mathrm{e}^{\mathrm{i}\alpha(y-ct)}], \tag{2.12}$$

$$\Psi=\Psi_B(x,t)+\epsilon\,\mathrm{Re}\,[\psi(x)\,\mathrm{e}^{\mathrm{i}\alpha(y-ct)}], \tag{2.13}$$

where $\Psi$ is the stream function defined by

$$u=\frac{\partial\Psi}{\partial y}, \quad v=-\frac{\partial\Psi}{\partial x}, \tag{2.14}$$

with $\Psi_B$ the basic solution corresponding to $v_B$ and $\bar{t}=t-t_0$ is the time measured

relative to a fixed time $t_0 > 0$. We seek travelling wave solutions, consistent with observation, such that the wavenumber $\alpha$ is real and $c$ is complex. By assuming that $\bar{t} \ll t_0$ the base flow functions $T_B$, $\bar{\Psi}_B$ and $v_B$ are evaluated in the stability analysis at time $t_0$, equivalent to a quasi-steady approximation in which the time scale for tracking the disturbance is assumed short compared with the time scale for the growth of the boundary layer. This effectively means that in forming the stability equations the time $t$ (which is retained in place of $t_0$) becomes a parameter of the problem and the linearized equations for the perturbation functions $\psi(x)$ and $\tau(x)$ in (2.13) and (2.12) are obtained as

$$\psi^{\mathrm{iv}} - 2\alpha^2\psi'' + \alpha^4\psi - \mathrm{i}\alpha[(v_B - c)(\psi'' - \alpha^2\psi) - v_B''\psi] + Pr^{-1}\tau' = 0, \tag{2.15}$$

$$\tau'' - \alpha^2\tau - \mathrm{i}\alpha\, Pr[(v_B - c)\tau - T_B'\psi] = 0, \tag{2.16}$$

where primes denote differentiation with respect to $x$. The boundary conditions are

$$\psi = \psi' = \tau = 0 \quad \text{at} \quad x = 0, \tag{2.17}$$

$$\psi, \psi', \tau \to 0 \quad \text{as} \quad x \to \infty. \tag{2.18}$$

The system (2.15)–(2.18) is an eigenvalue problem for the complex eigenfunctions $\psi$ and $\tau$, with complex eigenvalue $c = c_r + \mathrm{i}c_i$ for a given wavenumber $\alpha$. The only parameters in the problem are the Prandtl number $Pr$ and the non-dimensional time $t$, which is contained in the base flow functions $v_B$ and $T_B$. For fixed $Pr$ therefore, the control parameter is $t$.

## 3. The small-wavenumber limit

The eigenvalues obtained by solution of (2.15)–(2.18) give the relationship between the wavenumber, the wave speed and the amplification of travelling waves in the boundary layer. Some numerical solutions of the system have been previously obtained (e.g. Armfield & Patterson 1992) but as discussed above there is particular interest in the properties of the eigenvalues at small wavenumber, in the vicinity of the neutral curve. The results obtained by Armfield & Patterson (1992, figure 11) indicate that for small wavenumbers the left-hand branch of the neutral curve in the $(t, \alpha)$-plane asymptotes towards the $\alpha$-axis, corresponding to large values of the parameter $t$.

In the limit as $t \to \infty$, the main features of long-wavelength disturbances are described by a boundary-layer approximation to the stability equations in which

$$\alpha = t^{-2}\tilde{\alpha}, \quad c = t\tilde{c} + t^{-1/2}\tilde{c}_1 + \ldots. \tag{3.1}$$

Here the scaling of $c$ with $t$ is dictated by the requirement that wave speeds are comparable with the speed of the boundary layer, while the scaling of $\alpha$ ensures that viscous effects remain important. The need for a correction term in $c$ of relative order $t^{-3/2}$ will become apparent below. On the lateral scale of the boundary layer, defined by the coordinate $\eta = x/t^{1/2}$ the eigenfunctions $\psi$ and $\tau$ may be expanded as $t \to \infty$ in the form

$$\psi = \tilde{\psi}(\eta) + t^{-3/2}\tilde{\psi}_1(\eta) + \ldots, \quad \tau = t^{-3/2}\tilde{\tau}(\eta) + t^{-3}\tilde{\tau}_1(\eta) + \ldots. \tag{3.2}$$

The scaling of $\tau$ ensures that thermal effects are incorporated in a consistent manner.

Substitution into (2.15) and (2.16) shows that at leading order $\tilde{\psi}$ and $\tilde{\tau}$ satisfy the reduced system of equations

$$\tilde{\psi}^{\mathrm{iv}} - \mathrm{i}\tilde{\alpha}[(V - \tilde{c})\tilde{\psi}'' - V''\tilde{\psi}] + Pr^{-1}\tilde{\tau}' = 0, \tag{3.3}$$

$$\tilde{\tau}'' - \mathrm{i}\tilde{\alpha}\, Pr[(V - \tilde{c})\tilde{\tau} - F'\tilde{\psi}] = 0, \tag{3.4}$$

where primes now denote differentiation with respect to $\eta$. At the wall it follows from the full boundary conditions (2.17) that

$$\tilde{\psi} = \tilde{\psi}' = \tilde{\tau} = 0 \quad \text{at} \quad \eta = 0, \tag{3.5}$$

while at the outer edge, the boundary conditions become

$$\tilde{\psi}' \to 0, \quad \tilde{\tau} \to 0 \quad \text{as} \quad \eta \to \infty. \tag{3.6}$$

This outer condition requires some discussion. Equations (3.3) and (3.4) admit six possible behaviours as $\eta \to \infty$, two of which correspond to the linear form

$$\tilde{\psi} \sim b\eta + a \quad \text{as} \quad \eta \to \infty, \tag{3.7}$$

and the other four of which are of exponential form. Two of the exponential forms are

$$(\tilde{\psi}, \tilde{\tau}) \sim c^{\pm}(1, \mp Pr\,\lambda(\lambda^2 + \mathrm{i}\tilde{\alpha}\tilde{c}))\, \mathrm{e}^{\pm\lambda\eta}, \tag{3.8}$$

where

$$\lambda = (\tilde{\alpha}\,|\tilde{c}|\,Pr)^{1/2}\,[\cos(\tfrac{1}{2}\tilde{\theta} - \tfrac{1}{4}\pi) + \mathrm{i}\sin(\tfrac{1}{2}\tilde{\theta} - \tfrac{1}{4}\pi)], \tag{3.9}$$

with $\tilde{c} = \tilde{c}_r + \mathrm{i}\tilde{c}_i$, $\tilde{\theta} = \arctan(\tilde{c}_i/\tilde{c}_r)$; $|\tilde{\theta}| < \frac{1}{2}\pi$. The other two exponential solutions are defined by

$$(\tilde{\psi}, \tilde{\tau}) \sim d^{\pm}(1, 0)\, \mathrm{e}^{\pm\lambda\eta}, \tag{3.10}$$

where $\lambda$ is defined by (3.9) with $Pr$ set to unity; $a, b, c^{\pm}$ and $d^{\pm}$ are constants.

For general complex values of $\tilde{c}$, the boundary conditions (3.6) are equivalent to the specification $b = c^{+} = d^{+} = 0$ so that solutions which grow linearly or exponentially are excluded. This implies that the solution of equations (3.3) and (3.4) may be expected to have the behaviour

$$\tilde{\psi} \to a \quad \text{as} \quad \eta \to \infty, \tag{3.11}$$

whereas for the full stability problem $\psi \to 0$ at the outer edge. The explanation for the apparent discrepancy lies in the existence of an inviscid region outside the boundary layer where variations occur on a lateral scale comparable with the disturbance wavelength. Here the appropriate lateral coordinate is

$$\zeta = x/t^2 \tag{3.12}$$

and as $t \to \infty$,

$$\psi = \hat{\psi}(\zeta) + \ldots, \tag{3.13}$$

with the perturbation to the temperature field exponentially small. Equation (2.15) becomes $\hat{\psi}'' - \tilde{\alpha}^2\hat{\psi} = 0$ and the solution which matches with the behaviour (3.11) and decays to zero as $\zeta \to \infty$ is

$$\hat{\psi} = a\, \mathrm{e}^{-\tilde{\alpha}\zeta}. \tag{3.14}$$

Note that had the linear form (3.7) been allowed with $b \neq 0$ then a solution would have been required with $\hat{\psi} = 0$ at $\zeta = 0$, which would have resulted in exponential growth as $\zeta \to \infty$.

Apart from providing justification for the form of the outer boundary conditions for the reduced problem, the outer region also provides a correction to the growth rate and phase speed which is larger than that arising from the terms neglected in the stability equations. Since $\hat{\psi} = a - a\tilde{\alpha}\zeta + O(\zeta^2)$ as $\zeta \to 0$, it follows that the correction terms $\tilde{\psi}_1$ and $\tilde{\tau}_1$ in (3.2) must satisfy the boundary conditions

$$\tilde{\psi}_1' \to -a\tilde{\alpha}, \quad \tilde{\tau}_1 \to 0 \quad \text{as} \quad \eta \to \infty. \tag{3.15}$$

Thus the equations

$$\tilde{\psi}_1^{\mathrm{iv}} - \mathrm{i}\tilde{\alpha}[(V - \tilde{c})\,\tilde{\psi}_1'' - V''\tilde{\psi}_1] + Pr^{-1}\tilde{\tau}_1' = -\mathrm{i}\tilde{\alpha}\tilde{c}_1\,\tilde{\psi}'', \tag{3.16}$$

$$\tilde{\tau}_1'' - \mathrm{i}\tilde{\alpha}\,Pr\,[(V - \tilde{c})\,\tilde{\tau}_1 - F'\tilde{\psi}_1] = -\mathrm{i}\tilde{\alpha}\,Pr\,\tilde{c}_1\,\tilde{\tau} \tag{3.17}$$

must be solved subject to (3.15) and the wall conditions

$$\tilde{\psi}_1 = \tilde{\psi}_1' = \tilde{\tau}_1 = 0 \quad \text{at} \quad \eta = 0. \tag{3.18}$$

It is readily established that a solution exists only if $\tilde{c}_1$ is determined by the condition

$$\tilde{c}_1 \int_0^\infty (\bar{\psi}''\tilde{\psi} + Pr\,\bar{\tau}\tilde{\tau})\,\mathrm{d}\eta = \tilde{\alpha}a\tilde{c}\bar{\psi}(\infty), \tag{3.19}$$

where $\bar{\psi}$ and $\bar{\tau}$ are solutions to the adjoint system

$$\bar{\psi}^{\mathrm{iv}} - \mathrm{i}\tilde{\alpha}[(V-\tilde{c})\,\bar{\psi}]'' + \mathrm{i}\tilde{\alpha}[V''\bar{\psi} + Pr\,F'\bar{\tau}] = 0, \tag{3.20}$$

$$\bar{\tau}'' - \mathrm{i}\tilde{\alpha}\,Pr\,(V-\tilde{c})\,\bar{\tau} - Pr^{-1}\,\bar{\psi}' = 0, \tag{3.21}$$

with

$$\bar{\psi} = \bar{\psi}' = \bar{\tau} = 0 \quad \text{at} \quad \eta = 0, \tag{3.22}$$

$$\bar{\psi}' \to 0, \quad \bar{\tau} \to 0 \quad \text{as} \quad \eta \to \infty. \tag{3.23}$$

It has been shown in this section that as $t \to \infty$ long-wave disturbances develop a double-deck structure consisting of an inner region of thickness $x \sim t^{1/2}$, comparable with the width of the boundary layer, where the streamwise disturbance velocity is of order $\epsilon t^{-1/2}$ and a much wider isothermal outer region of thickness $x \sim t^2$, comparable with the wavelength of the instability, where the disturbance velocity of order $\epsilon t^{-2}$ generated at the edge of the inner layer decays to zero. The key properties of the instability are determined from the coupled system (3.3)–(3.6) governing the velocity and temperature fields of the disturbance in the inner region and solutions of this system are considered next.

## 4. Solution of the reduced stability equations

Numerical and asymptotic methods have been used to obtain solutions to the reduced system of equations (3.3) and (3.4). Numerical solutions were obtained independently by two different methods. The first method was based on outward integration of the equations from $\eta = 0$ to an outer boundary $\eta = \eta_\infty$ using a first-order Euler scheme along with an orthonormalization procedure (Davey 1973) to maintain accuracy. The asymptotic form of the outer boundary conditions was used to speed up convergence and reduce the dependence on the value of $\eta_\infty$. The system of equations is sixth order, and a $6 \times 6$ transfer matrix can be formulated; this can be reduced in the usual way to a $3 \times 3$ matrix, the determinant of which must vanish to ensure a non-trivial solution for the eigenfunctions. The vanishing of this determinant determines the values of $\tilde{c}_r$ and $\tilde{c}_i$ for a given value of $\tilde{\alpha}$.

The second method used a more accurate fourth-order Runge–Kutta scheme to integrate the equations inwards from $\eta_\infty$ to the wall. Here three solutions were computed corresponding to the behaviour defined by (3.7), (3.8) and (3.10) with $a$, $c^-$ and $d^-$ non-zero respectively. A linear combination of these and application of the boundary conditions at $\eta = 0$ leads to a complex $3 \times 3$ determinant whose zeros were located using a Newton iteration procedure.

Results from these two procedures were found to be in excellent agreement for the primary mode of instability, with the Euler method performing better at large values of $\tilde{\alpha}$ and the Runge–Kutta scheme better at small and moderate $\tilde{\alpha}$. The secondary modes were mostly calculated with the Runge–Kutta scheme, but could equally well have been obtained with the Euler method. Numerical accuracy checks consisted of varying the step size in $\eta$ and the value of $\eta_\infty$; in general a step size of $\Delta\eta = 0.02$ and

an outer boundary of $\eta_\infty = 30$ were found to be sufficient for the Runge–Kutta scheme, although at small $\tilde{\alpha}$ it was sometimes necessary to increase the value of $\eta_\infty$. It was also necessary to extend the outer boundary for the calculations at small $Pr$ described in §7.

A further check on the numerical solutions is provided by an analytical solution which can be obtained in the asymptotic limit as $\tilde{\alpha} \to \infty$. Here the effects of viscosity and thermal conductivity are confined mainly to the vicinity of a critical layer surrounding the location $\eta = \eta_m$ of the maximum base flow velocity in the boundary layer, and the phase speed of the disturbance approaches the maximum flow speed $V = V_m$, a feature of long-wave instabilities identified by Drazin & Howard (1962, §6) in the context of unbounded parallel inviscid flow. This behaviour was confirmed by Gill & Davey (1969) for the small-wavenumber limit of the Rayleigh equation governing inviscid disturbances in vertically stratified boundary layers and leads to a solution in which the perturbation field is negligibly small in the region $\eta < \eta_m$. A similar structure applies here as $\tilde{\alpha} \to \infty$ although solutions of the reduced system (3.3)–(3.6) do not match directly to solutions of a Rayleigh equation at higher wavenumbers but to those of an intermediate-wavenumber regime which will be discussed in detail in a later paper.

It is assumed that as $\tilde{\alpha} \to \infty$

$$\tilde{c} = c_0 + \tilde{\alpha}^{-1/2} c_1 + \tilde{\alpha}^{-3/4} c_2 + \dots, \tag{4.1}$$

and that in the region $\eta > \eta_m$

$$\tilde{\psi} = \psi_0(\eta) + \tilde{\alpha}^{-1/2}\psi_1(\eta) + \tilde{\alpha}^{-3/4}\psi_2(\eta) + \dots, \tag{4.2}$$

$$\tilde{\tau} = \tau_0(\eta) + \tilde{\alpha}^{-1/2}\tau_1(\eta) + \tilde{\alpha}^{-3/4}\tau_2(\eta) + \dots. \tag{4.3}$$

Substitution into (3.3) and (3.4) gives the inviscid approximations

$$(V - c_0)\,\psi_0'' - V''\psi_0 = 0, \quad (V - c_0)\,\tau_0 - F'\psi_0 = 0. \tag{4.4}$$

The requirement that $\psi_0$ remains finite as $\eta \to \infty$ implies that $\psi_0 = V - c_0$, where the multiplicative constant is taken as unity without loss of generality, and it follows that $\tau_0 = F'$. The value of $c_0$ is fixed by the requirement that $\psi_0$ vanishes at $\eta = \eta_m$, giving $c_0 = V_m$. Higher-order terms in (4.2) and (4.3) can be found in a straightforward manner. Making use of the requirement that $\tilde{\psi}$ remains finite as $\eta \to \infty$ and applying the normalization $\tilde{\psi}(\infty) = -\tilde{c}$ implies that $\psi_1 = -c_1$, $\psi_2 = -c_2$. In the vicinity of $\eta_m$, the base flow velocity can be expanded in the form

$$V = V_m - (\eta - \eta_m)^2 V_1 + \dots, \tag{4.5}$$

where $V_1 = -\frac{1}{2}V''(\eta_m) > 0$, and so

$$\psi_0 \sim -V_1(\eta - \eta_m)^2, \quad \tau_0 \to F_1 \quad \text{as} \quad \eta \to \eta_m, \tag{4.6}$$

where $F_1 = F'(\eta_m)$.

Locally the solution is modified within a critical layer whose lateral scale $\xi$ is determined by the need for viscosity and thermal conduction to be significant. Thus

$$\eta = \eta_m + \tilde{\alpha}^{-1/4}\xi \tag{4.7}$$

and forms which match those in (4.6) as $\xi \to \infty$ are

$$\tilde{\psi} = \tilde{\alpha}^{-1/2}\phi(\xi) + \dots, \quad \tilde{\tau} = \theta(\xi) + \dots, \quad \tilde{\alpha} \to \infty. \tag{4.8}$$

Substitution into (3.3) and (3.4) shows that $\phi$ and $\theta$ satisfy

$$\phi^{\mathrm{iv}} + \mathrm{i}[(V_1\xi^2 + c_1)\,\phi'' - 2V_1\xi\phi] = 0, \tag{4.9}$$

$$\theta'' + \mathrm{i}\,Pr\,[(V_1\xi^2 + c_1)\,\theta + F_1\phi] = 0 \tag{4.10}$$

and matching with the outer solution (4.2) requires that

$$\phi \sim -V_1 \xi^2 - c_1 + o(\xi^{-1}), \quad \theta \to F_1 \quad \text{as} \quad \xi \to \infty. \tag{4.11}$$

Here it is noted that the complementary solution of (4.9) proportional to $\xi^{-1}$ as $\xi \to \infty$ must be excluded as it would not match with the outer form for $\psi_2$. Assuming that the disturbances die out as $\xi \to -\infty$, it is also required that

$$\phi \to 0, \quad \theta \to 0 \quad \text{as} \quad \xi \to -\infty. \tag{4.12}$$

The system for $\phi$ given by (4.9), (4.11) and (4.12) decouples from that for $\theta$ and determines the eigenvalue $c_1$, as follows. Equation (4.9) can be integrated once and the transformations

$$\phi = V_1^{1/2} \Phi(X), \quad c_1 = V_1^{1/2} C, \quad \xi = V_1^{-1/4} X \tag{4.13}$$

applied to obtain

$$\Phi''' + \mathrm{i}[(X^2 + C)\Phi' - 2X\Phi] = 0. \tag{4.14}$$

Defining $\Phi^{(1)}(X)$ as the solution in $X > 0$ which is exponentially small as $X \to \infty$, it follows that

$$\Phi = -X^2 - C + A\Phi^{(1)}(X), \quad X > 0; \qquad \Phi = B\Phi^{(1)}(-X), \quad X < 0 \tag{4.15}$$

and then continuity of $\Phi$, $\Phi'$ and $\Phi''$ at $X = 0$ leads to the requirement that $B = -A$ and $C\Phi^{(1)\prime\prime}(0) - 2\Phi^{(1)}(0) = 0$. Setting

$$C = \mathrm{e}^{\mathrm{i}\pi/4}\hat{C}, \quad X = \mathrm{e}^{\mathrm{i}\pi/8}\hat{X}, \quad \Phi^{(1)} = \hat{\Phi}(\hat{X}), \tag{4.16}$$

it follows that $\hat{C}$ are the real eigenvalues of the system

$$\hat{\Phi}''' - (\hat{X}^2 + \hat{C})\hat{\Phi}' + 2\hat{X}\hat{\Phi} = 0, \quad \hat{X} \geqslant 0, \tag{4.17}$$

$$\hat{C}\hat{\Phi}'' - 2\hat{\Phi} = 0, \quad \hat{X} = 0; \qquad \hat{\Phi} \sim \hat{X}^{-(\hat{C}+5)/2}\,\mathrm{e}^{-\hat{X}^2/2}, \quad \hat{X} \to \infty, \tag{4.18}$$

and these are determined as

$$\hat{C} = 1 - 4n, \quad n = 0, 1, 2, \ldots. \tag{4.19}$$

This analytical result has been obtained previously by Cowley, Hocking & Tutty (1985) in their examination of the stability of general boundary-layer profiles containing a point of zero shear away from a wall.

This produces a set of eigenvalues of the reduced system as $\tilde{\alpha} \to \infty$ which is essentially independent of the thermal perturbation field, the critical layer solution for $\theta$ in (4.10) being generated by the known stream-function perturbation $\phi$. However, another set of eigenvalues exists associated with a set of thermal modes described by an alternative balance to (4.8) in which

$$\tilde{\psi} = \tilde{\alpha}^{-1/2}\phi(\xi) + \ldots, \quad \tilde{\tau} = \tilde{\alpha}^{1/4}\theta(\xi) + \ldots, \quad \tilde{\alpha} \to \infty. \tag{4.20}$$

In this case $\phi$ and $\theta$ satisfy the system

$$\theta'' + \mathrm{i}\,Pr\,(V_1 \xi^2 + c_1)\theta = 0, \tag{4.21}$$

$$\phi^{\mathrm{iv}} + \mathrm{i}[(V_1 \xi^2 + c_1)\phi'' - 2V_1\phi] + Pr^{-1}\theta' = 0 \tag{4.22}$$

and the size of $\tilde{\tau}$ in (4.20) now requires that the thermal field decays in both directions. Such solutions can be found by applying the transformations

$$\theta = V_1^{1/2} Pr^{-1/2}\Theta(X), \quad c_1 = V_1^{1/2} Pr^{-1/2} C, \quad \xi = V_1^{-1/4} Pr^{-1/4} X, \tag{4.23}$$

to obtain

$$\Theta'' + \mathrm{i}(X^2 + C)\Theta = 0; \quad \Theta \to 0, \quad X \to \pm\infty. \tag{4.24}$$

Defining $\Theta^{(1)}$ as the solution which is exponentially small as $X \to \infty$ it follows that

$$\Theta = A\Theta^{(1)}(X), \quad X > 0; \qquad \Theta = B\Theta^{(1)}(-X), \quad X < 0 \tag{4.25}$$

and continuity of $\Theta$ and $\Theta'$ at $X = 0$ leads to two possibilities; either $A = B$ and $\Theta^{(1)\prime}(0) = 0$, or $A = -B$ and $\Theta^{(1)}(0) = 0$. Setting

$$C = \mathrm{e}^{\mathrm{i}\pi/4}\hat{C}, \quad X = \mathrm{e}^{\mathrm{i}\pi/8}\hat{X}, \quad \Theta^{(1)} = \hat{\Theta}(\hat{X}) \tag{4.26}$$

then shows that $\hat{C}$ are the real eigenvalues of the system

$$\hat{\Theta}'' - (\hat{X}^2 + \hat{C})\,\hat{\Theta} = 0, \quad \hat{X} \geqslant 0, \tag{4.27}$$

$$\hat{\Theta} = 0 \quad \text{or} \quad \hat{\Theta}' = 0, \quad \hat{X} = 0; \qquad \hat{\Theta} \sim \hat{X}^{(1-\hat{C})/2}\,\mathrm{e}^{-\hat{X}^2/2}, \quad \hat{X} \to \infty. \tag{4.28}$$

The required solutions are

$$\hat{\Theta} = U(\tfrac{1}{2}\hat{C}, \sqrt{2}\hat{X}), \tag{4.29}$$

where $U$ is the parabolic cylinder function (see, for example, Abramowitz & Stegun 1965, p. 687), and where

$$\hat{C} = -1 - 2n, \quad n = 0, 1, 2, \ldots. \tag{4.30}$$

With $c_1$ determined, equation (4.22) now determines the stream-function perturbation $\phi$, subject to the boundary conditions for $\phi$ given by (4.11) and (4.12).

In summary, two sets of asymptotic solutions of the reduced system exist as $\tilde{\alpha} \to \infty$ and have growth rates and phase speeds determined by

$$\text{I:} \quad \tilde{c} \sim V_m + (V_1/2)^{1/2}(\mathrm{i}+1)(1-4n)\,\tilde{\alpha}^{-1/2}, \quad n = 0, 1, 2, \ldots, \tag{4.31}$$

$$\text{II:} \quad \tilde{c} \sim V_m - (V_1/2Pr)^{1/2}(\mathrm{i}+1)(1+2n)\,\tilde{\alpha}^{-1/2}, \quad n = 0, 1, 2, \ldots. \tag{4.32}$$

It is noted that only the leading branch ($n = 0$) of family I has $\tilde{c}_i > 0$ and therefore corresponds to a disturbance with positive growth rate; this is also the only disturbance for which the phase speed $\tilde{c}_r$ is greater than the maximum flow speed of the boundary layer.

## 5. Numerical results for the small-wavenumber limit

Numerical solutions of the reduced system (3.3) and (3.4) have been obtained for water ($Pr = 7.5$) and air ($Pr = 0.71$) over a wide range of wavenumbers. For other Prandtl numbers, the calculations focused on obtaining the dependence of the maximum phase speed and the wavenumber of neutral stability as a function of Prandtl number. Figures 1(*a*) and 1(*b*) show the real and imaginary parts of $\tilde{c}$ as a function of $\tilde{\alpha}$, for $Pr = 7.5$, for both families of disturbances, with $n = 0, 1$ for family I, and $n = 0, 1, 2, 3, 4$ for family II. Figure 1(*a*) shows that the maximum scaled phase speed achieved is $\tilde{c}_r = 0.0142$, at $\tilde{\alpha} = 91.1$, and is, consistently with the observations, greater than the maximum scaled boundary layer speed $V_m = 0.00795$ by a factor of almost two. From figure 1(*b*), the position of neutral stability, where $\tilde{c}_i = 0$, occurs at $\tilde{\alpha} = 139.5$, greater than the value for maximum phase speed. Positive growth rates occur only for this $n = 0$ mode for family I, and only for values of $\tilde{\alpha}$ greater than the neutral stability value. All phase speeds for $n > 0$ in family I, and for all $n$ in family II, are less than the maximum flow velocity for all values of $\tilde{\alpha}$. The growth rates for these cases are also negative.

Also in figure 1 are shown as dashed lines the asymptotic solutions ($\tilde{\alpha} \to \infty$) for each of the modes. These are clearly in good agreement with the computed values, even for relatively small values of $\tilde{\alpha}$. The $n = 0$ mode of family I has been computed out to $\tilde{\alpha} = 2 \times 10^4$, and the solution lies almost exactly on the asymptotic value.

At the other extreme, all of the solution branches were found to terminate at a finite

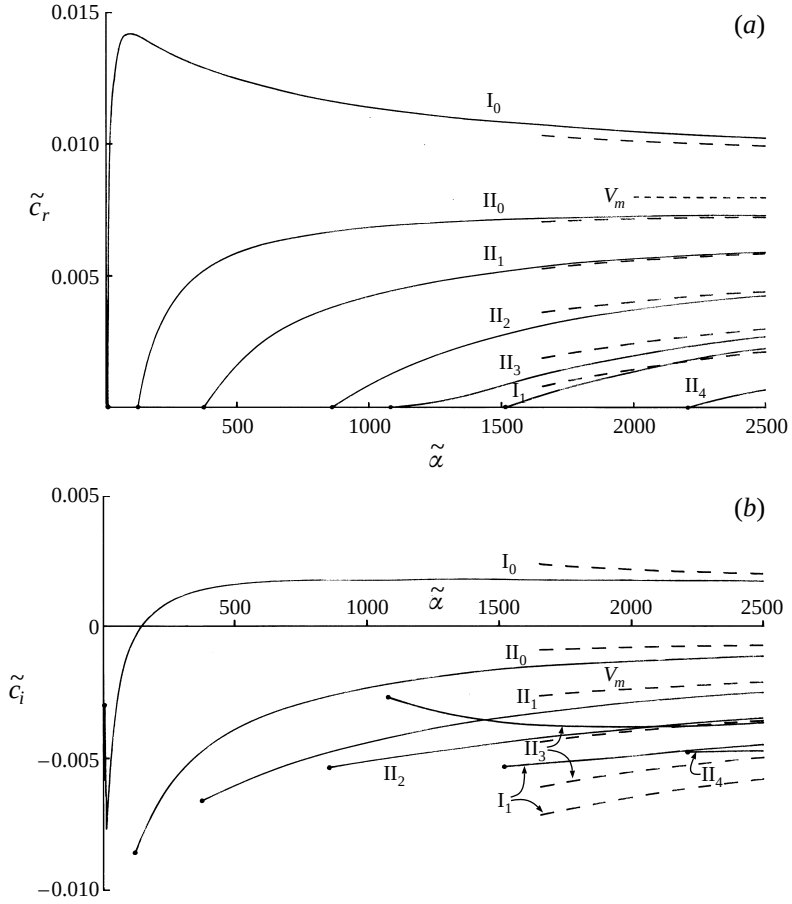


FIGURE 1. The eigenvalues (*a*) $\tilde{c}_r$ and (*b*) $\tilde{c}_i$ as a function of $\tilde{\alpha}$ for the reduced problem with $Pr = 7.5$. In each case, the solid line is the result of the numerical solution of the reduced set of equations, and the dashed line the asymptotic value for $\tilde{\alpha} \to \infty$. Modes $I_0$, $I_1$, $II_0$, $II_1$, $II_2$, $II_3$ and $II_4$ are shown. $V_m$ is the maximum boundary layer velocity.

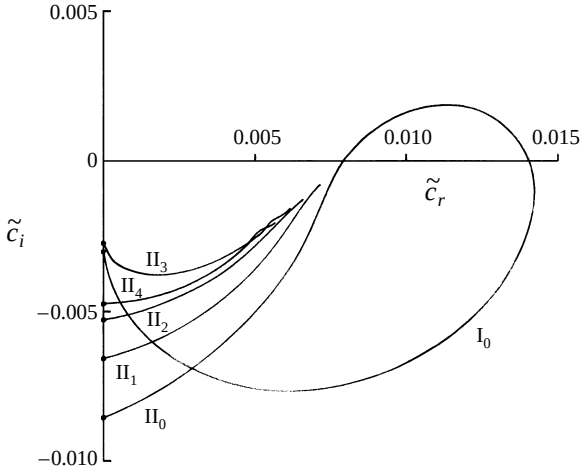


FIGURE 2. The eigenvalues for the modes $I_0$, $II_0$, $II_1$, $II_2$, $II_3$ and $II_4$ in the complex $\tilde{c}$-plane for $Pr = 7.5$.

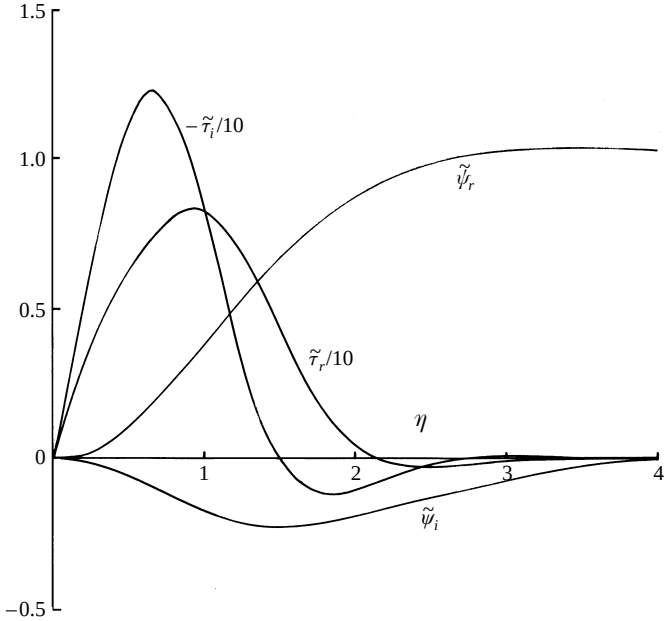


FIGURE 3. The real and imaginary components of the stream function and temperature eigensolutions as a function of distance from the wall for $Pr = 7.5$, evaluated at the neutral value of $\tilde{\alpha}$.

non-zero value of $\tilde{\alpha}$ where the phase speed $\tilde{c}_r$ becomes zero, and the growth rate approaches a finite negative value. As $\tilde{c}_r \to 0$, the exponential decay associated with (3.8) and (3.10) is lost in favour of an oscillatory behaviour when $\tilde{c}_r = 0$, so that the boundary condition (3.6) can no longer be satisfied. The loss at sufficiently small wavenumbers of solutions that decay across the boundary layer is perhaps not surprising; it is readily established from (3.3) and (3.4) that such solutions do not exist with $\tilde{\alpha}\tilde{c}$ finite when $\tilde{\alpha} = 0$, although solutions with bounded behaviour as $\eta \to \infty$ always exist provided $\tilde{c}_i < 0$.

The behaviour of the real and imaginary parts of $\tilde{c}$ is summarized in figure 2, which shows the paths of the various modes in the complex $\tilde{c}$-plane, each path asymptoting to a line drawn at 45° through the position $\tilde{c}_r = V_m$ on the real axis.

Figure 3 shows the real and imaginary parts of the eigenfunctions at the neutral stability point $\tilde{\alpha} = 139.5$, normalized so that $\tilde{\psi}(\infty) = 1$. The eigenfunctions have a similar shape at the position of maximum phase speed.

## 6. Solution of the full stability equations

The full stability system (2.15)–(2.18) has been solved for a range of values of the control parameter $t$, using the Euler method referred to above. Again, asymptotic boundary conditions are used to ensure convergence of the solution for reasonable values of an outer boundary $x = x_\infty$, particularly at small $\alpha$. Only the case $Pr = 7.5$ has been solved.

It is straightforward to show that as $x \to \infty$ for fixed $t$ the solutions to equations (2.15) and (2.16) must behave as

$$\psi \sim A\, e^{\lambda_1 x} + B\, e^{\lambda_2 x} + C\, e^{\lambda_3 x}, \tag{6.1}$$

$$\tau \sim e^{\lambda_1 x}, \tag{6.2}$$

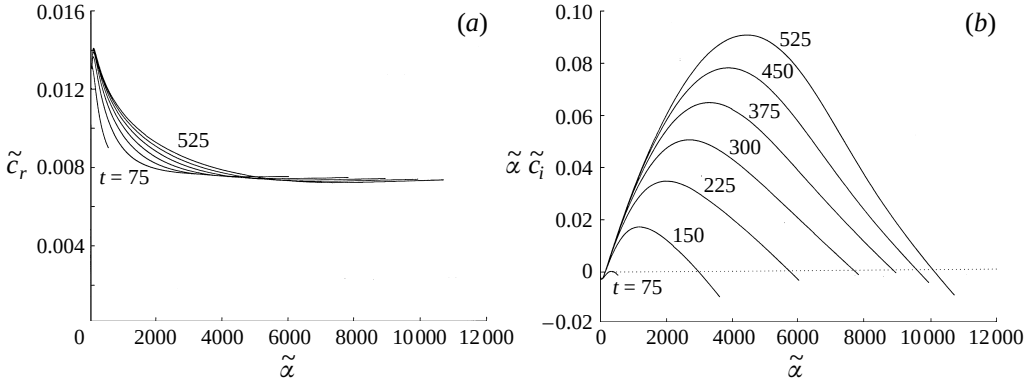


FIGURE 4. (*a*) The eigenvalues $\tilde{c}_r$ and (*b*) the amplification $\tilde{\alpha}\tilde{c}_i$ as functions of $\tilde{\alpha}$ for the full stability problem with $Pr = 7.5$. The various curves are for different values of the control parameter $t$ ranging from 75 to 525 in increments of 75. Only family I results are shown.

where $\lambda_1$ is the root of $\lambda_1^2 - \alpha^2 + \mathrm{i}\alpha\, Pr\, c = 0$ with negative real part, $\lambda_2 = -\alpha$ and $\lambda_3$ is the root of $\lambda_3^2 - \alpha^2 + \mathrm{i}\alpha c = 0$ with negative real part; in (6.1), $B$ and $C$ are arbitrary constants and $A$ is given by

$$A = \frac{-\lambda_1}{Pr\,(\lambda_1^4 - 2\alpha^2\lambda_1^2 + \alpha^4 + \mathrm{i}\alpha c(\lambda_1^2 - \alpha^2))}. \tag{6.3}$$

Consequently, the boundary conditions for (2.15) and (2.16) enforced as $x \to \infty$ are

$$\tau' - \lambda_1 \tau = 0, \tag{6.4}$$

$$\psi'' - (\lambda_1 + \lambda_2)\,\psi' + \lambda_2\lambda_3\,\psi - A(\lambda_1^2 - \lambda_1(\lambda_2 + \lambda_3) + \lambda_2\lambda_3)\,\tau = 0, \tag{6.5}$$

$$\psi''' - (\lambda_1 + \lambda_2 + \lambda_3)\,\psi'' + (\lambda_1\lambda_2 + \lambda_2\lambda_3 + \lambda_3\lambda_1)\,\psi' - \lambda_1\lambda_2\lambda_3\,\psi = 0. \tag{6.6}$$

The results of these computations are shown in figures 4(*a*) and 4(*b*) for a range of values of $t$. In these figures, the results are plotted in terms of the reduced system variables, rather than the variables defined in §2, for consistency. Figure 4(*a*) shows the value of $\tilde{c}_r$ as a function of $\tilde{\alpha}$, and figure 4(*b*) the amplification, given by $\tilde{\alpha}\tilde{c}_i$, for values of $t$ which increase from a value for which only a very small wavenumber range is unstable, $t = 75$, to $t = 525$, in increments of 75. The first value is close to the usual critical value for which an instability is first available. These figures show that the peak phase speed occurs for wavenumbers less than the lowest neutral wavenumber at all values of $t$ computed. Further, the individual plots appear to coincide at small $\tilde{\alpha}$, consistent with the $t^{-2}$ scaling (3.1). Only the main mode of instability has been calculated over the full range of values of $\tilde{\alpha}$.

Figures 5(*a*) and 5(*b*) show these results plotted on an expanded scale in the region appropriate to the reduced problem. Here, the dashed lines are the solutions to the reduced problem for those modes shown. Only the first modes from families I and II have been calculated and are shown in these figures; it is clear that, for these modes, at small wavenumber the solutions of the full stability problem collapse on to the solution of the reduced problem, confirming the indication suggested above. Some additional solutions for other modes have also been calculated and again coincide with the reduced problem solutions, but are not shown here.

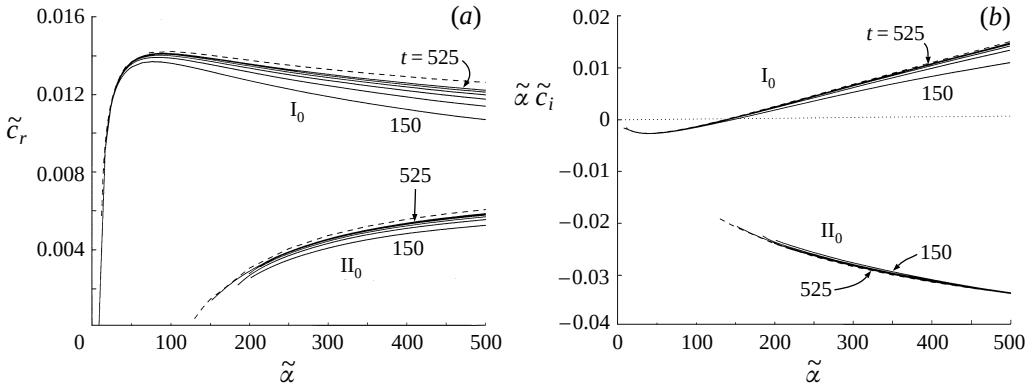


FIGURE 5. (*a*) Values of $\tilde{c}_r$ and (*b*) the amplification $\tilde{\alpha}\tilde{c}_i$ as functions of $\tilde{\alpha}$ (solid lines) for the full stability problem with $Pr = 7.5$ in a smaller range of $\tilde{\alpha}$, for modes $I_0$ and $II_0$, and for the range $t = 150$ to $t = 525$. The dashed line in each family is the corresponding solution to the reduced problem.

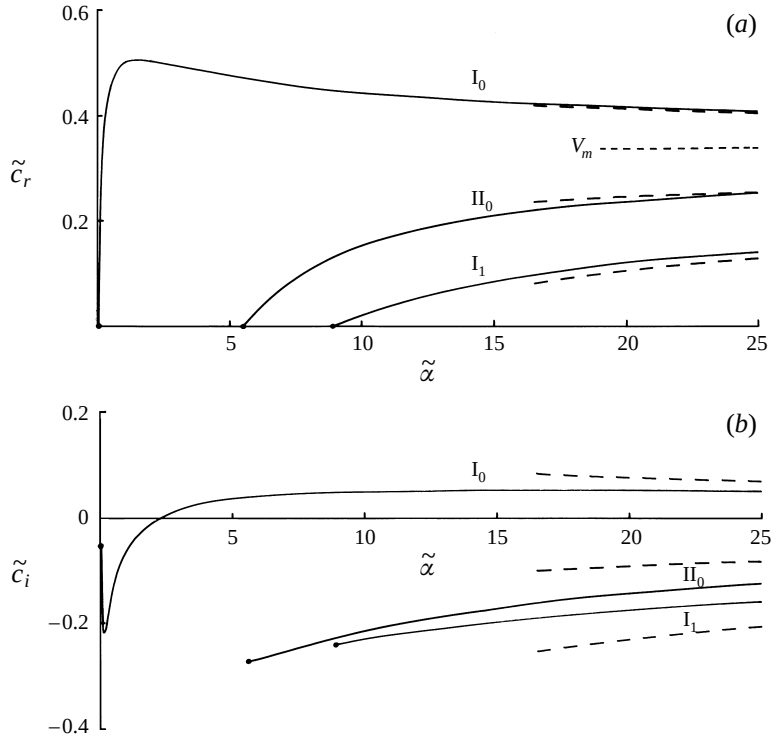


FIGURE 6. The dependence of (*a*) $\tilde{c}_r$ and (*b*) $\tilde{c}_i$ on $\tilde{\alpha}$ for the first few modes of the reduced problem for the case $Pr = 0.71$.

## 7. Dependence on Prandtl number

As indicated above, some numerical solutions of the reduced problem have been obtained for air ($Pr = 0.71$). The dependence of $\tilde{c}_r$ and $\tilde{c}_i$ on $\tilde{\alpha}$ for the first few modes is shown in figures 6(*a*) and 6(*b*). The results are qualitatively similar to those for $Pr = 7.5$, but with the thermal modes more suppressed, consistent with the inverse dependence on $Pr^{1/2}$ in the asymptotic form (4.32).

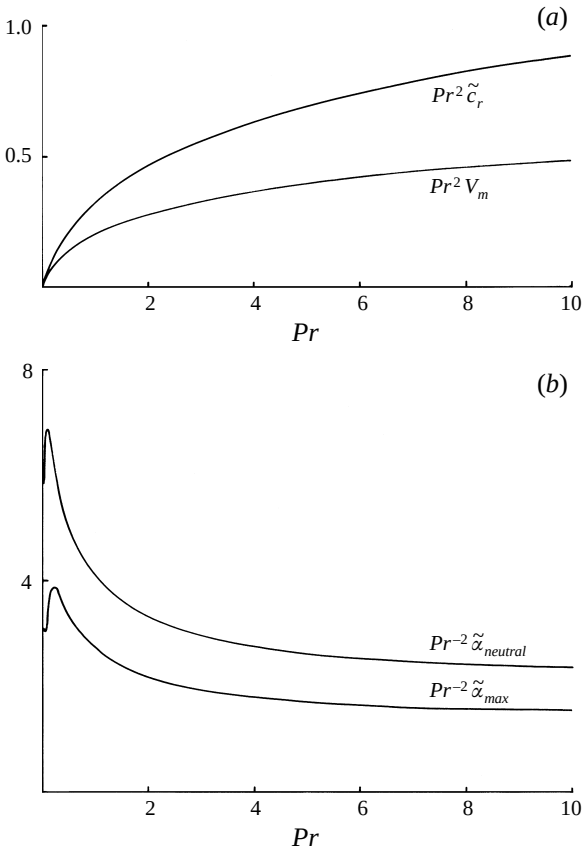


FIGURE 7. The variation with $Pr$ of (*a*) the maximum value of $Pr^2\tilde{c}_r$ and (*b*) the maximum phase speed and neutral values of $Pr^{-2}\tilde{\alpha}$ for the leading mode of the reduced problem.

Figures 7(*a*) and 7(*b*) show the dependence of the main properties of the reduced system on the Prandtl number, obtained for the range $0.02 \leqslant Pr \leqslant 10$. From figure 7(*a*) it is seen that the ratio of the maximum phase speed to the maximum boundary layer velocity is not constant, but varies over a relatively small range, 1.29 at $Pr = 0.1$ to 1.81 at $Pr = 10$. A similarly small change in the ratio between the values of $\tilde{\alpha}$ for maximum phase speed and for neutral conditions is evident in figure 7(*b*). For $Pr$ less than about 0.2, the variation in this ratio is relatively large, but for $Pr > 0.5$ the ratio is consistently close to 0.66. Evidently the behaviour of the reduced stability system is qualitatively similar over a wide range of Prandtl numbers so long as the Prandtl number is not too small.

## 8. Discussion

An investigation of the stability properties of the natural-convection boundary layer on a doubly infinite vertical plate was prompted by the numerical and experimental observations of travelling wave groups on the starting flow following sudden heating of a vertical wall, both in the context of the semi-infinite plate and cavity flows. An analysis of the stability properties at low wavenumber has shown that the peak phase speed always occurs at a wavenumber less than the neutral value; that is, the fastest travelling waves are decaying. Further, the peak velocity is greater than the fastest

velocity available in the boundary layer by a factor of about two. As the wavenumber increases in the primary mode of instability, the phase speed in this low-wavenumber approximation approaches the maximum boundary layer velocity from above, i.e., the phase speed is always greater than the boundary layer velocity, but asymptotes towards it with increasing wavenumber.

The model for the 'leading-edge effect' put forward by Armfield & Patterson (1992) suggested that the effect consisted of this group of waves, with the deviation from the purely one-dimensional solution at a particular point beginning as the fastest wave passes that point, followed by the spectrum of amplified waves. Thus the deviation should be seen at a speed consistent with the fastest phase speed, and the following oscillatory signal should be visible as the most-amplified wave in the amplified spectrum. Although the latter condition cannot be confirmed with the present low-wavenumber analysis, certainly the indications are that the fastest wave speed is of the right order to match the experimental and numerical observations.

The group velocity of the travelling wave spectrum is given by

$$v_g = \frac{\partial \omega}{\partial \alpha}, \tag{8.1}$$

where $\omega$ is the frequency, given by $\omega = \alpha c_r$. Thus $v_g = c_r + \alpha\, \partial c_r/\partial \alpha$. At the peak phase velocity, $v_g = c_r$, and at the neutral point $v_g$ is only slightly less than the maximum phase velocity since $\partial c_r/\partial \alpha$ is small for $\alpha$ greater than the value for the maximum phase velocity. The maximum group velocity occurs for values of $\alpha$ less than the value of maximum phase velocity, where the amplification is negative. From figures 1(*a*) and 1(*b*), the first amplified wavenumber when $Pr = 7.5$ corresponds to $\tilde{\alpha} = 140$ and the group velocity at this wavenumber is given by $v_g = 0.0133t$, compared with a peak phase speed of $0.0142t$ and a peak boundary layer velocity of $0.008t$.

Although the primary purpose of this paper is to establish the stability properties of the thermal boundary layer at low wavenumber and not to expand on the leading-edge effect, it is of interest to compare these values of velocity, i.e., the maximum phase velocity and the first amplified group velocity, with the values estimated for the speed of the leading-edge effect from Armfield & Patterson (1992). They obtained numerical results for Boussinesq flow in a rectangular cavity of height $H$ and temperature difference $\Delta T_H$ between the two sidewalls using a finite difference scheme with third-order upwind differencing of the convective terms and a Crank–Nicolson time integration. Their results for a Rayleigh number $Ra = g\beta \Delta T_H H^3/\nu\kappa$ can be compared with the present theory by noting that $\Delta T_H = 2\Delta T$ so that $h/H = (Ra/2)^{-1/3}$, where $h$ is defined in §2. For a square cavity at mid-height with $Ra = 6 \times 10^8$, $Pr = 7.5$ and $t^* = 4.7 \times 10^{-4} H^2/\nu$ they estimated the speed of the leading-edge effect to be $v^* = 2.2 \times 10^3 \nu/H$. Given that for these parameter values $t = t^*\nu/h^2 = 2.11 \times 10^2$, this corresponds in the present scaling to a non-dimensional vertical speed $v = v^*h/\nu$ of $0.0156t$, which compares favourably with the peak phase speed $0.0142t$ quoted above. Recent experiments on a semi-infinite plate by Graham (1995), also for $Pr = 7.5$, give a corresponding value, again in the present scaling, of $0.0139t$.

A number of other non-amplifying modes have also been revealed in the analysis of the small-wavenumber-limit problem. Although these evidently play no role in the transition of the boundary layer, they are relevant in the sense that it has been possible to show that the primary mode is the only mode which has any amplified spectrum, and is also the only mode in which the wave speeds are greater than the base flow maximum velocity for any value of wavenumber.

The information lacking in the present analysis involves the properties at larger

wavenumbers, and specifically the properties of the amplified spectrum. Although we are able to obtain this numerically, as shown in figures 4(*a*) and 4(*b*), it is also possible to obtain more detailed analytical results. As mentioned previously, small-wavenumber results discussed here do not directly match the lower asymptotic limit of the accompanying Rayleigh problem associated with finite wavenumbers, and a third intermediate-wavenumber regime is required. All of the modes identified here may be shown to match across these three regimes, and the solutions to the full stability equations to collapse on to the limiting results when the appropriate scalings are applied. This will be the topic of a future paper. It is also hoped to address the more difficult question of how the analysis could be improved to take proper account of the temporal evolution of the basic state and its effect on both the stability of the flow and the propagation of the leading-edge effect. Here we have focused on the temporal stability problem on the grounds that at a given instant the disturbance is first manifest as a wave travelling on the one-dimensional boundary-layer flow which is, therefore, equally susceptible at any vertical location. However, in reality any disturbance generated near the leading edge will amplify or decay both spatially and temporally, suggesting that the results of a spatial stability analysis may also be of interest. Another natural convective boundary layer flow where the present methods can be applied is the buoyancy layer studied by Gill & Davey (1969). This stratified flow is relevant to the steady-state structure that evolves in laterally heated cavities and in this case the present method should lead to the determination of the peak phase velocity of long-wave disturbances without the need to incorporate any quasi-steady assumption.

This work was begun while J. C. P. was visiting City University, and completed while P. G. D. was visiting the University of Western Australia. The project has been supported by the UK Engineering and Physical Sciences Research Council under grant no. GR/J93788, and the Australian Research Council under grants no. A89331991 and A89532739. Their support is gratefully acknowledged. Useful conversations with Wolfgang Schöpf, Steve Armfield and Andrew Brooker are also acknowledged.

## REFERENCES

Abramowitz, M. & Stegun, I. A. 1965 *Handbook of Mathematical Functions*. Dover.

Armfield, S. W. & Patterson, J. C. 1992 Wave properties of natural convection boundary layers. *J. Fluid Mech.* **239**, 195–211.

Brown, S. N. & Riley, N. 1973 Flow past a suddenly heated vertical plate. *J. Fluid Mech.* **59**, 225–237.

Cowley, S. J., Hocking, L. M. & Tutty, O. R. 1985 The stability of solutions of the classical unsteady boundary-layer equation. *Phys. Fluids* **28**, 441–443.

Davey, A. 1973 A simple numerical method for solving Orr–Sommerfeld problems. *Q. J. Mech. Appl. Maths* **24**, 401–410.

Drazin, P. G. & Howard, L. N. 1962 The instability to long waves of unbounded parallel inviscid flow. *J. Fluid Mech.* **14**, 257–283.

Gebhart, B. & Mahajan, R. L. 1982 Instability and transition in buoyancy induced flows. *Adv. Appl. Mech.* **22**, 231–315.

Gill, A. E. & Davey, A. 1969 Instabilities of a buoyancy-driven system. *J. Fluid Mech.* **35**, 775–798.

Goldstein, R. J. & Briggs, D. G. 1964 Transient free convection about vertical plates and circular cylinders. *Trans. ASME J. Heat Transfer* **86**, 490–500.

Graham, T. 1995 Unsteady natural convection adjacent to a semi-infinite vertical plate. *Proc. 12th Australasian Fluid Mechanics Conference, Sydney*.

Ingham, D. B. 1985 Flow past a suddenly heated vertical plate. *Proc. R. Soc. Lond.* A **402**, 109–134.

Joshi, Y. & Gebhart, B. 1987 Transition of vertical natural convection flows in water. *J. Fluid Mech.* **179**, 407–438.

Krane, M. J. M. & Gebhart, B. 1993 The hydrodynamic stability of a one-dimensional transient buoyancy induced flow. *Intl J. Heat Mass Transfer* **36**, 977–988.

Mahajan, R. L. & Gebhart, B. 1978 Leading edge effect in transient natural convection flow adjacent to a vertical surface. *Trans. ASME J. Heat Transfer* **100**, 731–733.

Ostrach, S. 1964 Laminar flows with body forces. In *Theory of Laminar Flows* (ed. F. K. Moore), pp. 528–718. Princeton University Press.

Schladow, S. G. 1990 Oscillatory motion in a side heated cavity. *J. Fluid Mech.* **213**, 589–610.

Siegel, R. 1958 Transient free convection from a vertical flat plate. *Trans. ASME J. Heat Transfer* **80**, 347–359.